The Journal of Chemical Physics

Lattice-gas model of a charge regulated planar surface

Cite as: J. Chem. Phys. **154**, 074706 (2021); https://doi.org/10.1063/5.0039029
Submitted: 30 November 2020 . Accepted: 14 January 2021 . Published Online: 17 February 2021

Daniel Alejandro Gomez, Derek Frydel, and Yan Levin

The Journal of Chemical Physics ARTICLE scitation.org/journal/jcp

Lattice-gas model of a charge regulated planar surface

Cite as: J. Chem. Phys. 154, 074706 (2021); doi: 10.1063/5.0039029
Submitted: 30 November 2020 • Accepted: 14 January 2021 •
Published Online: 17 February 2021

Daniel Alejandro Gomez,[1] Derek Frydel,[1,a)] and Yan Levin[2]

AFFILIATIONS

[1] Department of Chemistry, Federico Santa Maria Technical University, Campus San Joaquin, Santiago, Chile
[2] Institute of Physics, The Federal University of Rio Grande do Sul, Porto Alegre 91501-970, Brazil

[a)] **Author to whom correspondence should be addressed:** dfrydel@gmail.com

ABSTRACT

In this work, we consider a lattice-gas model of charge regulation with electrostatic interactions within the Debye–Hückel level of approximation. In addition to long-range electrostatic interactions, the model incorporates the nearest-neighbor interactions for representing non-electrostatic forces between adsorbed ions. The Frumkin–Fowler–Guggenheim isotherm obtained from the mean-field analysis accurately reproduces the simulation data points.

I. INTRODUCTION

If we overlook the difference of length scales, the physical context, and other circumstantial details, then it is not difficult to see analogy between a system of interfacial colloids[1–6] and a system of chemically active surfaces.[7–21] The analogy is, in particular, true with regard to electrostatics, in which case, using the relatively well-known understanding of electrostatics of interfacial colloids can be transferred to the problem of charge regulation.

In the case of interfacial colloids, nano-sized colloidal particles are permanently trapped at an interface between two immiscible fluids, such as air–water or oil–water interface, due to capillary and electrostatic interactions.[1] In the case of charge regulation, surface ionic groups dissociate from a surface or associate onto it as a result of quantum mechanical interactions.[7,12,14,17] The common feature in the two systems is an interface.

The understanding of electrostatics of interfacial colloids goes back to 1961 and the work of Stillinger,[2] who obtained an expression for an electrostatic potential of a point charge near an interface within linear electrostatics. Stillinger pointed out the existence of an effective repulsive interaction between a charge and an interface. Twenty four years later, Hurd[3] pointed out another interesting feature of charges at an interface; the interaction between surface charges is not screened monopole-like, but at large separations, it becomes unscreened and dipole-like.

In this work, we consider a lattice-gas (LG) model of charge regulation that builds on those basic results. In previous articles,[17,19] we provided phenomenological expressions, primarily based on the mean-field (MF) analysis, for a surface charge of a simulated microscopic model of sticky-charged hard-spheres that represent surface chemical groups. As the simulation data are limited, the range of validity of those expressions could not be fully verified. Working with a LG model and linear electrostatics provides a simpler and a more tractable system. Simulation results are easily available as the bulk part of the system is implicit in the parameters of the LG model and does not need to be simulated. The linear treatment of electrostatics permits the superposition of various contributions of interactions. The approximate expressions can be easily tested and compared to simulation results for a range of different parameters. The LG model permits us, furthermore, to incorporate short-range nearest-neighbor (NN) interactions and study their effect on charge regulation.

This paper is organized as follows. In Sec. II, we introduce a sticky site meant to represent a covalent bond between an ion and a surface chemical group. In Sec. III, we discuss contributions of electrostatics within the Debye–Hückel (DH) approximation. In Sec. IV, we formulate the lattice-gas (LG) model of charge regulation for basic chemical groups. In Sec. V, we consider the mean-field (MF) approximation and the self-consistent Frumkin–Fowler–Guggenheim isotherm for the average occupation of a site.

In Sec. VI, we discuss the simulation results. In Sec. VII, we consider the LG model for acidic surface groups. In Sec. VIII, we finish with concluding remarks.

II. STICKY SITE

A. In a bulk solution

To model the formation of a chemical bond between a lattice site of the LG model and an approaching molecule, we use the sticky site potential $u_s(r)$ whose Boltzmann factor is a delta function,[15–17,19,22]

$$e^{-\beta u_s(|\mathbf{r}-\mathbf{r}_s|)} = 1 + v_s\delta(\mathbf{r}-\mathbf{r}_s), \tag{1}$$

and v_s is the stickiness of a lattice site. By representing the sticky site as a spherical well potential of radius Δ and depth ε, the stickiness can be represented as $v_s = \frac{4\pi\Delta^3}{4}e^{\beta\varepsilon}$, assuming $\Delta \to 0$.

Introducing a sticky site at the location $\mathbf{r}_s$ modifies the original partition function Z as

$$Z' = \frac{1}{N!\Lambda^{3N}}\int d\mathbf{r}_1 \ldots \int d\mathbf{r}_N\, e^{-\beta U} e^{-\beta\sum_{i=1}^{N} u_s(|\mathbf{r}_i-\mathbf{r}_s|)}, \tag{2}$$

where $U(\mathbf{r}_1, \ldots, \mathbf{r}_N)$ is the remaining part of the configurational potential. The Boltzmann factor of the sticky potential can be expanded as

$$e^{-\beta\sum_{i=1}^{N} u_s(|\mathbf{r}_i-\mathbf{r}_s|)} = 1 + v_s\sum_{i=1}^{N}\delta(\mathbf{r}_i-\mathbf{r}_s) + \cdots, \tag{3}$$

but since a sticky site can be occupied by at most one particle at a time, only the first two terms of the expansion are relevant, and the partition function becomes

$$Z' = Z[1 + v_s\rho(\mathbf{r}_s)], \tag{4}$$

where Z is the partition function of the original system and $\rho(\mathbf{r}_s) = \sum_{i=1}^{N}\langle\delta(\mathbf{r}_s-\mathbf{r}_i)\rangle$ is the local density. Based on the above result, the probability that a sticky site is occupied can be expressed as

$$p \equiv \langle n\rangle = \frac{v_s\rho(\mathbf{r}_s)}{1 + v_s\rho(\mathbf{r}_s)}. \tag{5}$$

The above result is essentially a Langmuir isotherm.[23]

B. At a planar surface

If a sticky site is brought to a planar surface, the geometric restriction of the new configuration is expected to reduce the site stickiness (or the reactivity of a chemical group). By representing a sticky site as a spherical well potential in the zero size limit, it could easily be seen how the planar interface eliminates one half of the well potential so that $v_s^{surf} = v_s/2$.[17,19] Within the collision theory of a reaction mechanism, the reduced reactivity of a surface group may be seen as a result of a complete elimination of collisions coming from the other side of a wall.

More generally, the contributions of geometric confinement[24] can be represented by a dimensionless geometric factor g^{surf},

$$v_s^{surf} = g^{surf} v_s.$$

For the case at hand, we assume $g^{surf} = 1/2$.

If a planar surface is at $x = 0$, the probability that a site is occupied is

$$p = \frac{v_s g^{surf}\rho(0)}{1 + v_s g^{surf}\rho(0)}, \tag{6}$$

where $\rho(0)$ is a local density at the location of a wall.

C. v_s as the equilibrium constant of a reaction in a bulk

A bare sticky site represents a basic chemical group, and the empty/occupied site represents a de-protonated/protonated chemical group in accordance with the following chemical reaction:[17,19]

$$\mathrm{B} + \mathrm{H}^+ \rightleftharpoons \mathrm{BH}^+, \tag{7}$$

characterized by the concentration-based equilibrium constant defined as

$$K_b = \frac{c_{\mathrm{BH}^+}}{c_{\mathrm{H}^+}c_{\mathrm{B}}}, \tag{8}$$

where c_i is the concentration of species i in the aqueous solution.

If prior to the dissolution of B the concentrations are $c_{\mathrm{B}} = c$ and $c_{\mathrm{BH}^+} = c_{\mathrm{H}^+} = 0$, then at equilibrium, these concentrations are

$$\begin{aligned} c_{\mathrm{BH}^+} + c_{\mathrm{B}} &= c, \\ c_{\mathrm{BH}^+} &= cp, \\ c_{\mathrm{B}} &= c(1-p), \end{aligned} \tag{9}$$

where p is the probability that a single molecule B (or a sticky site) is protonated (occupied). Replacing the concentrations in K_b with those in (9) yields

$$K_b = \frac{p}{1-p}\frac{1}{c_{\mathrm{H}^+}}. \tag{10}$$

Using Eq. (5) for p with $\rho(\mathbf{r}_s) = c_{\mathrm{H}^+}$ leads to

$$p = \frac{v_s c_{\mathrm{H}^+}}{1 + v_s c_{\mathrm{H}^+}} \quad \to \quad \frac{p}{1-p}\frac{1}{c_{\mathrm{H}^+}} = v_s. \tag{11}$$

A comparison of Eq. (10) with Eq. (11) leads to a straightforward identity,

$$K_b = v_s. \tag{12}$$

The probability that a molecule is protonated can now be expressed as

$$p = \frac{K_b c_{\mathrm{H}^+}}{1 + K_b c_{\mathrm{H}^+}}, \tag{13}$$

which is the Langmuir isotherm for a reaction in a bulk.

One common basic molecule is ammonia, $\mathrm{B} = \mathrm{NH_3}$, with $K_b = 1.8 \times 10^9 \mathrm{M}^{-1}$. In the nanometer units, this corresponds to the stickiness parameter $v_s = 3.0 \times 10^9$ nm^3. A slightly larger methylamine, $\mathrm{B} = \mathrm{CH_3NH_2}$, yields $v_s = 7.6 \times 10^{10}$ nm^3.

In Refs. 17 and 19, we relate the surface stickiness to an equilibrium constant using a different procedure based on two alternative formulations of the virial expansion: physical and chemical. Within the chemical interpretation, the pair of particles that stick to one another is considered as a third species. The equality $v_s = K_b$ emerges by comparing the terms of the two expansions. The above procedure is more intuitive and straightforward.

III. ELECTROSTATICS

All electrostatic interactions and quantities in this work are treated on the DH level of approximation and follow from the formalism in Appendix A.

A. Distortion of a counterion cloud

The first contribution of electrostatic interactions is indirect and caused by distortion of a counterion cloud of an ion as it approaches a planar interface. The distortion lowers the solvation energy of an ion and gives rise to an effective repulsive interaction between a point charge and a wall. The repulsion, in turn, gives rise to an inhomogeneous density of ions (or protons in the case of acid–base reactions) near an interface,

$$\rho(x) = c_{\mathrm{H}^+} e^{-\beta w(x)}, \tag{14}$$

where c_{H^+} is the bulk concentration of protons related to pH as $c_{\mathrm{H}^+} = 10^{-p\mathrm{H}}$.

Within DH, $w(x)$ is known exactly.[2–6] If we ignore the dielectric discontinuity across the wall, $\epsilon = \epsilon_{in} = \epsilon_{out}$, where ϵ_{in} and ϵ_{out} are the dielectric constants inside and outside an electrolyte, then

$$\beta w(x) = \frac{\kappa\lambda_B}{2}\left[\frac{(1+\kappa x)^2 e^{-2\kappa x}}{2\kappa^3 x^3} - \frac{K_2(2\kappa x)}{\kappa x}\right], \tag{15}$$

where $K_2(x)$ is the Bessel function of the second kind. The expression is derived in Appendix B. Far away from a wall, $w(x)$ is dominated by an exponential decay, $\beta w(x) \approx \frac{1}{2}\frac{\lambda_B}{2x} e^{-2\kappa x}$, which suggests that a point charge interacts with its image charge on the other side of an interface at $x_{image} = -x$.

As $\kappa x < 1$, the functional form of $w(x)$ changes, and at the location of a wall, $\beta w(0) = \frac{\kappa\lambda_B}{6}$. The probability that a site is occupied, obtained using Eq. (6), can be expressed as

$$p = \frac{K_b c_{\mathrm{H}^+} g^{surf} e^{-\kappa\lambda_B/6}}{1 + K_b c_{\mathrm{H}^+} g^{surf} e^{-\kappa\lambda_B/6}}. \tag{16}$$

The above result is the Langmuir isotherm for a reaction at a surface. The equilibrium constant for this reaction is modified, with reference to the same reaction in a bulk, as

$$K_b^{surf} = K_b g^{surf} e^{-\kappa\lambda_B/6}. \tag{17}$$

Modifications are the result of geometric and electrostatic effects. Both contributions reduce the equilibrium constant. The expression does not take into account electrostatic interactions between adsorbed charges.

B. Direct electrostatic interactions

More relevant are the direct electrostatic interactions between adsorbed charges. If the dielectric discontinuity across a wall is ignored, the interaction between two point charges at a planar interface is[2–6]

$$\beta u(r) = \frac{2\kappa\lambda_B}{\kappa^3 r^3} - 2\kappa\lambda_B\left(\frac{1+\kappa r}{\kappa^3 r^3}\right)e^{-\kappa r}, \tag{18}$$

where the details of the derivation can be found in Appendix C. The interaction has two contributions, the screened negative interaction and the long-range dipole-like term, where the effective dipole moment is $\mu = 2^{1/2}\kappa^{-1}$. The dipole term arises as a result of anisotropic shape of counterion cloud, producing a perpendicular to a surface dipole moment.

IV. LG MODEL OF CHARGE REGULATION

In this section we define the LG model of charge regulation, that, because of linear electrostatics, is valid for weakly charged surfaces. The partition function governing the model is,

$$\Xi_{lg} = \sum_{n_1}\cdots\sum_{n_N} e^{-\beta H}, \tag{19}$$

where $n_i = 0, 1$ is the occupation number of lattice i and N is the total number of sites. The Hamiltonian of the system is defined as

$$H = \sum_{j>i}^{N} n_i n_j u(r_{ij}) - I\sum_{nn} n_i n_j - \mu\sum_{i=1}^{N} n_i, \tag{20}$$

where the chemical potential is given by

$$\beta\mu = \ln\left(g^{surf} v_s c_{\mathrm{H}^+}\right) - \frac{\kappa\lambda_B}{6}. \tag{21}$$

The electrostatic interaction between adsorbed protons has two contributions,

$$\beta u(r_{ij}) = 2\lambda_B\kappa\left[f_{dip}(\kappa r_{ij}) + f_{short}(\kappa r_{ij})\right],$$

given by

$$f_{dip}(x) = \frac{1}{x^3}, \quad f_{short}(x) = -\left(\frac{1+x}{x^3}\right)e^{-x}. \tag{22}$$

To generalize the model, we include the NN interactions, $I\sum_{nn} n_i n_j$, where the pair $\langle i, j\rangle$ are nearest neighbors.[25,26] For $I > 0$, these interactions are attractive and may represent hydrogen bonds between adsorbed groups or the weaker van der Waals interactions, and for $I < 0$, these interactions are repulsive and may represent overcrowding of larger chemical groups attached to a proton.

The simulated system is a two-dimensional LG model on a square-lattice. The simulation cell is a square of size $L = 64$. To incorporate the periodic boundary conditions, the interactions between sites i and j include the interactions between its images in different cells,

$$f^*(\kappa r_{ij}) = \sum_{m,n=-N_c}^{N_c} f\left(\kappa\sqrt{x_{ij} + maL)^2 + (y_{ij} + naL)^2}\right), \tag{23}$$

where $x_{ij} = x_i - x_j$ and $y_{ij} = y_i - y_j$ are respective separations between sites within a single simulation cell. N_c, in principle, is an infinite number, but we find that $N_c = 50$ is sufficiently large to exclude finite size effects. The function $f^*(\kappa r_{ij})$ is calculated only once during a simulation run.

A Monte Carlo move consists of a random selection of a lattice site followed by the trial change of its occupation; an occupied site is made empty, and an empty site is made occupied. The move is accepted if it lowers the energy; otherwise, it is accepted with the probability $e^{-\beta\Delta H}$.

A dipolar LG model has previously been studied in connection to Langmuir monolayers.[27–30] In the context of charge regulation, the possibility of a phase transition has recently been considered within the MF and field-theoretical methods.[31]

V. THE MEAN-FIELD APPROXIMATION

Within the MF, the interactions between particles can be incorporated into an effective chemical potential,

$$\beta\mu_{eff} = \beta\mu - p[\beta U - z\beta I],$$

where the quantity U is defined as

$$U = \sum_{j\neq i}^{N} u(r_{ij}) \tag{24}$$

and represents the electrostatic potential at a single site due to interactions with all other sites that are assumed to be occupied and z is the number of the nearest neighbors. The effective one-body Hamiltonian becomes

$$\beta H_{eff} = -\beta\mu_{eff}\sum_{i=1}^{N} n_i, \tag{25}$$

and the probability that a single site is occupied results in a self-consistent Frumkin–Fowler–Guggenheim isotherm[32,33] specific to our model,

$$p = \frac{e^{\beta\mu}e^{p\beta(zI-U)}}{1+e^{\beta\mu}e^{p\beta(zI-U)}}. \tag{26}$$

The above result treats short- and long-range interactions on the same level. The MF generally works well for long-range interactions.[34] On the other hand, for LG models, it is more of a qualitative tool that predicts the existence of a phase transition but is less accurate in predicting the exact critical point. Prior to seeing the results, it is not clear how the MF will handle the combination of short- and long-range interactions.

By representing the average magnetization of the Ising model in terms of p as $m = 2p - 1$,[35] Eq. (26) transforms into a familiar self-consistent relation,[36]

$$m = \tanh\left[\beta\left(\frac{2\mu + zI - U}{4}\right) + m\beta\left(\frac{zI-U}{4}\right)\right], \tag{27}$$

where $h = \mu/2 + (zI - U)/4$ is the external field and $J = (zI - U)/4$ is the interaction strength for the Ising model with the Hamiltonian $H_{Is} = h\sum_i s_i - J\sum_{nn} s_i s_j$. Equation (27) has a similar structure to that in Eq. (13) in Ref. 37 obtained within the field-theoretical formulation of charge regulation.

Equation (26) cannot be solved analytically, but by putting it into the form

$$xe^{x} + rx = n,$$

the solution can be identified as the generalized r-Lambert function $x = W_r(n)$.[38–41] Although it is possible to express $W_r(n)$ as a Taylor series, in practice, it is more convenient to calculate p numerically, especially, as deeper understanding of mathematical properties of the generalized r-Lambert function is not a closed project.[40,41]

To evaluate U, we use

$$\beta U = 2\kappa\lambda_B\left[\frac{M}{\kappa^3 a^3} - \sum_{i,j=0}^{\infty}{}' \frac{e^{-\kappa r_{ij}}(1+\kappa r_{ij})}{\kappa^3 r_{ij}^3}\right], \tag{28}$$

where M is the lattice sum (or the Madelung constant), which for parallel dipoles on a square and hexagonal lattice is[28]

$$M = \sum_{m,n=0}^{\infty}{}'\left(\frac{1}{m^2+n^2}\right)^{3/2} = 9.033\,622,$$

$$M = \sum_{m,n=0}^{\infty}{}'\left(\frac{1}{(m+n/2)^2+3n^2/4}\right)^{3/2} = 11.034\,176,$$

respectively. The summation in the second term is calculated explicitly due to its quick convergence and requires no more than a handful of the initial terms. The approximate analytical expression for U is provided in Appendix D.

VI. RESULTS

A. No nearest-neighbor interactions: $I = 0$

We consider first the case with the NN interactions switched off. In Fig. 1, we plot the occupation probability p as a function of pH for different salt concentrations. It compares the MF with the simulation data points. The first observation is that the MF accurately approximates the simulation results. Another observation is that the MF with the coarse-grained value of U (represented by thin dashed lines and derived in Appendix D) produces the results that are nearly indistinguishable from those obtained from the MF with exact U.

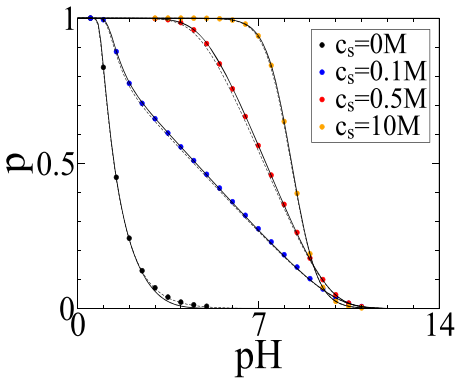

FIG. 1. The average occupation p as a function of pH for different salt concentrations c_s. The simulation data points (for a square-lattice substrate with lattice size $a = 0.6$ nm) are compared with the MF; the solid lines are for the MF with exact U, and thinner dashed lines are for the MF with a coarse-grained value of U. The system parameters are $K_b = \upsilon_s = 3 \times 10^9$ nm^3 and $\lambda_B = 0.72$ nm. The NN interactions are switched off, $I = 0$.

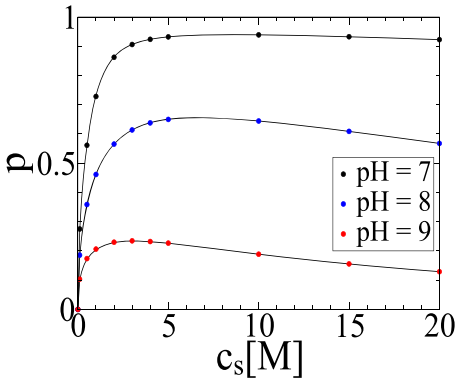

FIG. 2. The average occupation p as a function of c_s for different pH. The system's fixed parameters are $K_b = v_s = 3 \times 10^9$ nm^3 and $\lambda_B = 0.72$ nm. The simulation data points (for a square-lattice with $a = 0.6$ nm) are compared with the MF (solid lines).

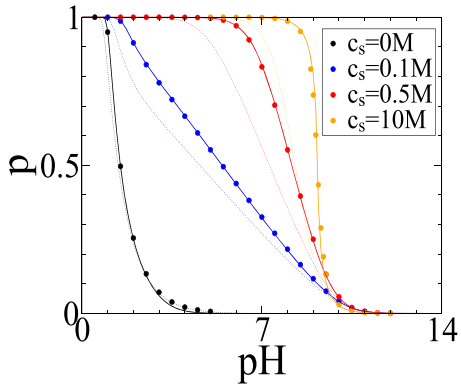

FIG. 4. The average occupation p as a function of pH for different concentrations of salt c_s. The system parameters are $K_b = v_s = 3 \times 10^9$ nm^3, $\lambda_B = 0.72$ nm, and $a = 0.6$ nm. The solid lines are for the MF for $\beta I = 1$, and the dashed lines are for the MF for $I = 0$.

We next turn to physical interpretation of the plots. For zero salt concentration, $c_s = 0$, there is no significant adsorption until only when the solution is strongly acidic, pH < 3. The addition of salt facilitates adsorption as a result of a more efficient screening of electrostatic interactions with other adsorbed protons. For example, for large salinity corresponding to the concentration $c_s = 10$M, the active sites are half-filled in a solution that is basic pH ≈ 9.

Screening of electrostatic interactions is not the sole consequence of increased salinity. Because increased salinity of a bulk solution leads to a more favorable solvation energy, the effect that is captured by the contribution $\beta w(0)$, it becomes increasingly more difficult for an ion to approach an interface.

In Fig. 2, we plot p as a function of c_s for different pH to get a more complete view of the effect of c_s on adsorption. All plots show the incipient sharp increase in p as a function of c_s. The increase, however, is not indefinite and for large salt concentrations p saturates and then slowly starts to decrease, reflecting the reduced μ with increased c_s.

In Fig. 3, we plot a couple of configuration snapshots for $c_s = 0$ where the electrostatic interactions are least screened. There is no visual indication of correlations or structural inhomogeneities that might arise as a result of dipolar repulsive interactions. This explains the accuracy of the MF approximation for this regime.

FIG. 3. Configuration snapshots of the LG model for $c_s = 0$M and pH = 1.2, 1.6 (all other parameters as in Figs. 1 and 2). The average occupation for those parameters roughly corresponds to $p \approx 0.4, 0.7$. The size of the simulation cell is $L = 64$, and so, the total number of lattice sites is $N = 64 \times 64$.

B. Attractive nearest-neighbor interactions: $I > 0$

Next, we consider the LG model with attractive NN interactions. In real systems, such attractive short-range interactions might arise due to hydrogen bonding between adsorbed groups.[8]

Figure (4) shows p as a function of pH for different values c_s and the interaction parameter $\beta I = 1$. All results are prior to phase transition. The simulation data points are accurately reproduced by the MF approximation (solid lines). In addition, we plot the MF results for $I = 0$ (dashed lines) for reference. The attractive NN interactions, as expected, facilitate adsorption, and all the curves are shifted toward higher pH.

The LG system with NN attractive interactions undergoes phase transition with the critical value of I given by[42]

$$\beta I_c = 2 \ln\left[1 + \sqrt{2}\right] = 1.762\,75\ldots. \tag{29}$$

The MF prediction of the critical value of I, obtained from Eq. (27), is

$$\beta I_c^{mf} = \frac{4}{z} = 1, \tag{30}$$

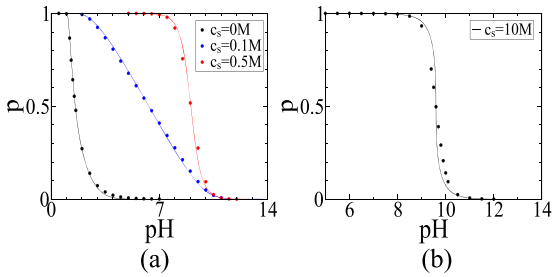

FIG. 5. Analogous plots to those in Fig. 4 but for $\beta I = 2$. The plot for $c_s = 10$M is shown separately as it is very close to the critical point.

FIG. 6. Configuration snapshots for c_s = 0.5M (pH = 9) and c_s = 2M (pH = 9.9) for attractive NN interactions for $\beta I = 2$.

which is considerably lower. In the presence of electrostatic interactions, I_c is shifted to higher values of I,

$$\beta I_c^{mf} = \frac{4}{z} + \frac{\beta U}{4}. \tag{31}$$

Although the MF is not exact, the trend predicted by it is reasonable. The result indicates that βI_c is shifted up by $\beta U/4$, and since U strongly depends on κ, this results indicates that the critical point can be regulated with salinity.

In Fig. 5, we make a plot similar to that in Fig. 4 but for $\beta I = 2$ and for $c_s < 1$ to ensure that electrostatic interactions are sufficiently strong to suppress phase transition driven by NN interactions. The MF theory continues to accurately reproduce the simulation data. The plot for c_s = 10M is shown separately as it is close to the critical point, where the MF starts to break down.

To visualize what is happening near the shifted critical point, in Fig. 6, we plot configuration snapshots for $\beta I = 2$ and c_s = 0.5M and c_s = 2M (and pH that roughly yields the occupation $p = 0.5$). As the repulsive electrostatic interactions become screened at higher salt concentration, the density fluctuations become stronger, indicating the closer vicinity of a critical point.

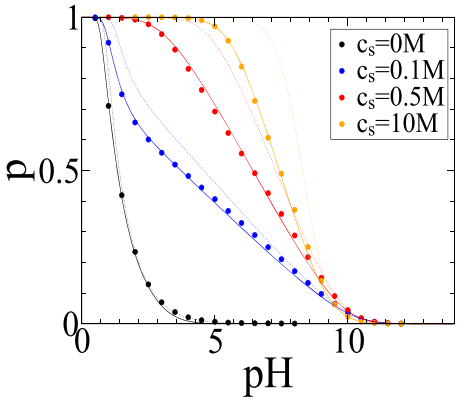

FIG. 7. The average occupation p as a function of pH for different salt concentrations c_s for the system with repulsive NN interactions corresponding to $\beta I = -1$. The remaining parameters are the same as those in Fig. 5. The solid lines are for the MF with $\beta I = -1$, and the dashed lines are for the MF with $I = 0$.

FIG. 8. Configuration snapshots for c_s = 0.5M and for pH = 5.5 and pH = 4 for repulsive NN interactions with $\beta I = -2$.

C. Repulsive nearest-neighbor interactions: $I < 0$

The repulsive NN interactions, which can represent the overcrowding effect of adsorbed molecules, are expected to reduce the occupation p. This is seen in Fig. 7, which plots p as a function of pH. The NN interactions are set at $\beta I = -1$. The MF (solid lines) accurately reproduces the simulated data points, and the comparison with the MF for $\beta I = 0$ indicates the shift toward lower pH.

The LG model with strictly NN repulsive interactions undergoes phase transition at the same critical value of βI as for the system with NN attractive interactions but an opposite sign. The strong repulsive interactions generate a configuration with every other site occupied, as seen in Fig. 8, but as the chemical potential increases, the repulsive interactions are eventually overcome and the empty sites become occupied. The point where this transpires corresponds to phase transition.

Both short- and long-range interactions in this case are repulsive, and the critical point within the MF is shifted according to

$$\beta I_c^{mf} = -\left(\frac{4}{z} - \frac{\beta U}{4}\right).$$

We recall that the MF does not distinguish between the short- and long-range interactions, so the formula above, although intuitively accurate, cannot be taken too "literally." For example, there is no evidence that the long-range repulsive interactions give rise to configurations and subsequently phase transition, seen in Fig. 8.

In Fig. 9, we plot p as a function of pH for $\beta I = -1.5$ and $\beta I = -2$. The results indicate a gradual breakdown of the MF as the

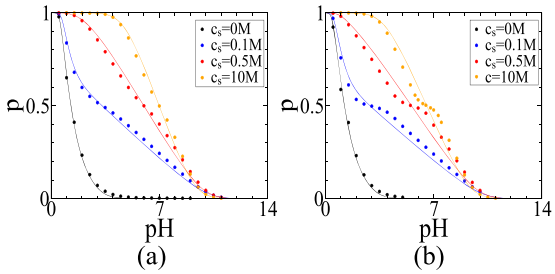

FIG. 9. p as a function of pH for different salt concentrations c_s for the system with repulsive NN interactions corresponding to (a) $\beta I = -1.5$ and (b) $\beta I = -2$. The remaining parameters are the same as those in Fig. 7.

system starts to phase separate. This is especially true for $\beta I = -2$, where the curves show a step-like structure, indicating a coexistence region.

VII. CHARGED STICKY SITES

In this section, we consider charged sticky sites to represent acidic chemical groups and the corresponding dissociation reaction,

$$\mathrm{HA} \rightleftharpoons \mathrm{A}^- + \mathrm{H}^+, \tag{32}$$

characterized by the concentration-based equilibrium constant given by

$$K_a = \frac{c_{\mathrm{H}^+} c_{\mathrm{A}^-}}{c_{\mathrm{AH}}}. \tag{33}$$

If the initial concentration of an acid HA prior to it being dissolved is c, then the equilibrium concentrations are given by

$$\begin{aligned} c_{\mathrm{HA}} + c_{\mathrm{A}^-} &= c, \\ c_{\mathrm{HA}} &= cp, \\ c_{\mathrm{A}^-} &= c(1-p), \end{aligned} \tag{34}$$

where p is the probability for an ion A^- to accept a proton. Inserting the above concentrations into Eq. (8) yields

$$K_a = \left(\frac{1-p}{p}\right) c_{\mathrm{H}^+}. \tag{35}$$

To complete the expression for K_a, we need an expression for p. However, in order to use Eq. (5), we need an expression for $\rho(\mathbf{r}_s)$. Because a sticky site is charged, the distribution of protons around it cannot be assumed to be uniform. In other words, $\rho(\mathbf{r}_s) \neq c_{\mathrm{H}^+}$.

For the time being, we postpone the question of the precise form of $\rho(\mathbf{r}_s)$ and assume the ansatz $\rho(\mathbf{r}_s) = c_{\mathrm{H}^+} e^{-\beta u_c}$, where u_c is the total effective potential at the location of a sticky site due to all electrostatic effects. This includes direct attractive interactions between a particle and a site and indirect repulsive interactions due to the less favorable solvation energy caused by distortion of counterions. Equation (5) then becomes

$$p = \frac{v_s c_{\mathrm{H}^+} e^{-\beta u_c}}{1 + v_s c_{\mathrm{H}^+} e^{-\beta u_c}} \quad \rightarrow \quad \frac{p}{1-p}\frac{1}{c_{\mathrm{H}^+}} = v_s e^{-\beta u_c}, \tag{36}$$

and the acid dissociation constant is

$$K_a = \frac{1}{v_s e^{-\beta u_c}}. \tag{37}$$

Going back to Eq. (36), we can now write

$$p = \frac{c_{\mathrm{H}^+}}{K_a + c_{\mathrm{H}^+}} \tag{38}$$

so that the occupation probability only depends on K_a and c_{H^+}, both experimentally accessible parameters.

To determine the quantity βu_c more precisely, we start by ignoring other ions in a solution so that βu_c is just the Coulomb attraction between a charged sticky site and an adsorbed ion, in which case, $\beta u_c = -\lim_{r\to 0} \lambda_B / r$. The problem with this expression is that βu_c diverges at the location of a sticky site. However, if the distance of the closest approach between two charges is $r = h$, then the Coulomb energy of an adsorbed charge would be

$$\beta u_c = -\frac{\lambda_B}{h}.$$

If a sticky site is immersed in an electrolyte, the contributions of other ions need to be included. We first assume the most simplest scenario where H^+ and A^- are point charges, and the adsorption occurs at a single point at separation h so that the associated molecule represents a dumbbell. Since the potential between two charges within the DH theory is $\beta e\psi(r) = -\lambda_B e^{-\kappa r} r^{-1}$, then

$$\beta u_c = -\frac{\lambda_B e^{-\kappa h}}{h}. \tag{39}$$

Because the point charges do not distort their respective counterion clouds, there is no repulsive effective interaction.

We can make the picture increasingly more realistic by assuming that an ion A^- is a spherical cavity immersed in an electrolyte, and the sticky site lies on the surface of a sphere. Within the DH, the Coulomb potential inside the cavity is shifted by a constant,[43] $\beta e\psi(r) = -\frac{\lambda_B}{r} + \frac{\kappa\lambda_B}{1+\kappa h}$, and the potential energy on a surface of a cavity is $\beta e\psi(r) = -\frac{\lambda_B}{h+\kappa h^2}$, in which case, for an associated molecule HA, we have

$$\beta u_c = -\frac{\lambda_B}{h + \kappa h^2} + \beta w_c, \tag{40}$$

where w_c is the work necessary to distort the counterion cloud around the point charge as it becomes adsorbed on a surface of a cavity. For large κ, the curvature of a spherical cavity can be ignored, and we could use the result for the planar wall $\beta w_c = \kappa\lambda_B/6$.

In Fig. 10, we plot the experimental data points for K_a as a function of the ionic strength[44] and compare it to the following expression:

$$K_a = \frac{e^{\beta w_c}}{v_s e^{\lambda_B/(h+\kappa h^2)}}, \tag{41}$$

obtained from Eq. (37) with u_c in Eq. (40) and $w_c = 0$, where the fitting parameter is h.

A. Charged sticky site at a planar surface

The acidic site is represented as a sticky site with a point charge displaced a distance h into a non-electrolyte phase. The electrostatic

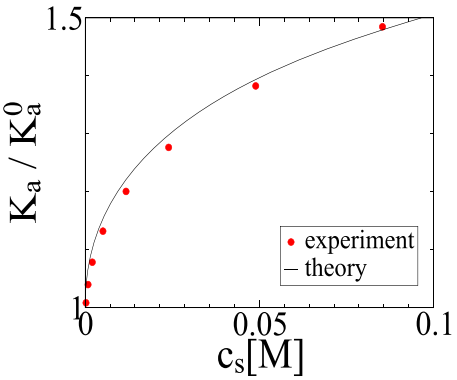

FIG. 10. Concentration-based equilibrium constant K_a as a function of c_s. The experimental data points are for the acetic acid CH_3COOH and the salt is NaCl.[44] The theoretical fit is for Eq. (41) with $\beta w_c = 0$ for $h = 0.8$ nm.

potential for this case within the DH theory is (see Appendix E)

$$\beta u_c(h) = \frac{\lambda_B}{h}\left[\pi(Y_2(\kappa h) - \boldsymbol{H}_2(\kappa h)) + 4\left(\frac{1}{\kappa h}\right)^2 + \frac{2}{3}\kappa h\right], \quad (42)$$

where $Y_2(x)$ is the Bessel function of the second kind and $\boldsymbol{H}_2(x)$ is the Struve function. The above expression is accurately approximated by the simple functional form,

$$\beta u_c(h) \approx -\frac{\lambda_B}{h + \kappa h^2/2}. \quad (43)$$

B. LG model for charged sticky sites

The Hamiltonian of the LG model for charged sticky sites is

$$H = \sum_{j>i}^{N}(1-n_i)(1-n_j)u(r_{ij}) - I\sum_{nn} n_i n_j - \mu\sum_{i=1}^{N} n_i. \quad (44)$$

Note that the electrostatic interactions are only between empty sites. The occupied charged sites are neutral.

The chemical potential of charged sticky sites is given by

$$\beta\mu = \ln\left(g^{surf} v_s c_{H^+}\right) - \frac{\kappa\lambda_B}{6} + \frac{\lambda_B}{h + \kappa h^2/2}, \quad (45)$$

where the last term is due to the direct electrostatic interaction between a charged site and an adsorbed particle as given in Eq. (43). After rearrangement, the chemical potential can be written as

$$\beta\mu = \ln\left(g^{surf} v_s e^{\lambda_B/h} c_{H^+}\right) - \frac{\kappa\lambda_B}{6}\left(\frac{4+\kappa h/2}{1+\kappa h/2}\right) \quad (46)$$

so that the κ-dependent terms are separated from the rest.

C. Results

For a charged sticky site, the self-consistent MF relation for p, analogous to that in Eq. (26) and corresponding to the Frumkin–Fowler–Guggenheim isotherm of our model, is given by

$$p = \frac{e^{\beta(\mu+U)} e^{p\beta(zI-U)}}{1 + e^{\beta(\mu+U)} e^{p\beta(zI-U)}}, \quad (47)$$

where μ is given in Eq. (46) and U in Eq. (24).

In Fig. 11, we plot p as a function of pH for charged sticky sites for different values of c_s. The results indicate that increased salinity reduces adsorption. This is in contrast to basic surface groups and is the result of more efficient screening of attractive electrostatic interactions between a proton and surface acidic groups.

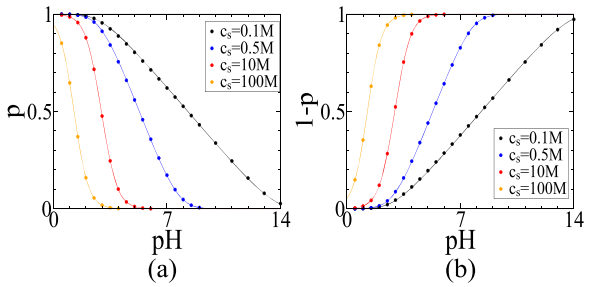

FIG. 11. p and $1-p$ as a function of pH for the surface with charged sticky sites and with no NN interactions. The simulation data points are compared with the MF (solid lines). The system parameters are λ_B = 0.72 nm, h = 0.2 nm, and $K_a^0 = 2.0\times10^{-5}\text{nm}^{-3}$.

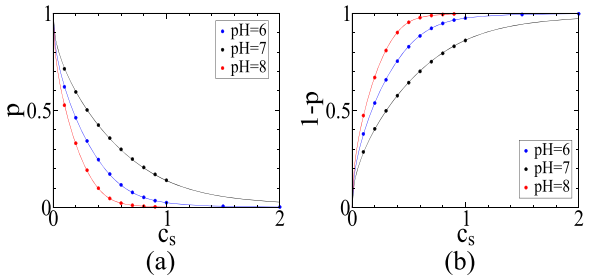

FIG. 12. p and $1-p$ as a function of c_s for different values of pH. The MF corresponds to solid lines. The remaining parameters are the same as in Fig. 11.

In Fig. 12, we plot p as a function of c_s. Unlike for acidic surface groups (see Fig. 2), the curves are monotonic for all values of c_s.

Because in the case of the acidic groups the surface charge is proportional to $1-p$,

$$\sigma_c = -(1-p)\sigma_A,$$

in Figs. 11 and 12, we plot $1-p$ to facilitate a comparison with the corresponding figures for basic groups in Figs. 1 and 2. For both basic and acidic surface groups, the surface charge increases with salinity. However, different trends emerge with respect to pH. In the case of basic groups, σ_c increases with pH, and in the case of acidic groups, σ_c decreases with pH.

VIII. CONCLUSION

In this work, we study the LG model of charge regulation within the DH approximation. The advantage of using DH is that the bulk part of the system is implicitly accounted for in the parameters of the model and can be left out from simulations. Furthermore, linear electrostatics permits the superposition of separate contributions to design more complex scenarios.

The separability of contributions provides an analytical advantage of breaking down observable properties into elements. For example, in the case of basic surface groups, the larger salinity lowers the solvation energy of a dissolved proton, which makes adsorption less favorable. However, instead, we see enhanced adsorption with increased salinity. This is because the larger salinity also happens to screen repulsive interactions between adsorbed protons, which, in fact, is a dominating contribution.

Although not explored in this work, the model could be specialized to represent more specific experimental situations. One could incorporate the dielectric discontinuity across an interface by using different expressions for $w(x)$ and $u(r)$,[2,3,6] for example, the dipolar part of interactions becomes modified by a factor $\epsilon_{out}/\epsilon_{in}$, or consider a more realistic lattice geometry, such as a triangular or a randomly distributed geometry.[45–47] Finally, but not last, one could consider charge regulation within a narrow confinement between two planar walls by using the relevant expressions for $w(x)$ and $u(r)$.

ACKNOWLEDGMENTS

D.F. acknowledges financial support from the FONDECYT through Grant No. 1201192. D.F. is thankful for private conversations with Anibal Valenzuela Sobarzo and acknowledges the University of Tel Aviv for invitation under the program the "Visiting Scholar of the School of Chemistry." D.G. acknowledges financial support from ANID/Scholarship Program/DOCTORADO BECAS CHILE through Grant No. 21201521.

APPENDIX A: DEBYE–HÜCKEL THEORY

In this section, we go over the DH formalism for a point charge in the vicinity of a planar insulator–electrolyte interface at $x = 0$ with an electrolyte at $x > 0$. If a point charge is located at $\mathbf{r}_0 = (x_0, 0, 0)$, then an electrostatic potential in each region is governed by the following two equations in cylindrical coordinates:

$$\begin{aligned} \nabla^2\phi(x>0,s) &= \kappa^2\phi(x,s) - 4\pi\lambda_B\frac{\delta(x-x_0)\delta(s)}{2\pi s}, \\ \nabla^2\phi(x<0,s) &= 0, \end{aligned} \tag{A1}$$

where $s = \sqrt{y^2+z^2}$ and $\phi = \beta e\psi$ is the dimensionless potential. The delta function $\delta(\mathbf{r} - \mathbf{r}_0)$ in cylindrical coordinates is $\delta(x - x_0)\delta(s)/2\pi s$. For the neutral wall, the boundary condition between the two regions is

$$\phi(0^-) = \phi(0^+), \quad \phi'(0^-) = \phi'(0^+).$$

Fourier transforming the equations in Eq. (E1) with respect to s,

$$\hat{\phi}(q,x) = 2\pi\int_0^\infty ds\, s J_0(qs)\phi(x,s), \tag{A2}$$

leads to

$$\begin{aligned} \hat{\phi}''(q,x) &= \left(\kappa^2+q^2\right)\hat{\phi}(q,x) - 4\pi\lambda_B\delta(x-x_0), \\ \hat{\phi}''(q,x) &= q^2\hat{\phi}(q,x). \end{aligned} \tag{A3}$$

The delta function splits the first region. The general solutions in each region are

$$\begin{aligned} \hat{\phi}(q,x>x_0) &= A_1 e^{-(x-x_0)\sqrt{\kappa^2+q^2}}, \\ \hat{\phi}(q,x<x_0) &= A_2 e^{(x-x_0)\sqrt{\kappa^2+q^2}} + B_2 e^{-(x-x_0)\sqrt{\kappa^2+q^2}}, \\ \hat{\phi}(q,x<0) &= A_3 e^{xq}. \end{aligned} \tag{A4}$$

The four coefficients A_1, A_2, B_1, and B_2 are determined from the boundary conditions. The continuity of the potential yields

$$\begin{aligned} A_1 &= A_2 + B_2, \\ A_3 &= A_2 e^{-x_0\sqrt{\kappa^2+q^2}} + B_2 e^{x_0\sqrt{\kappa^2+q^2}}, \end{aligned} \tag{A5}$$

and the continuity of the field yields

$$\begin{aligned} -A_1 &= A_2 - B_2 - \frac{4\pi\lambda_B}{\sqrt{\kappa^2+q^2}}, \\ A_3\frac{q}{\sqrt{\kappa^2+q^2}} &= A_2 e^{-x_0\sqrt{\kappa^2+q^2}} - B_2 e^{x_0\sqrt{\kappa^2+q^2}}, \end{aligned} \tag{A6}$$

and the coefficients are given by

$$\begin{aligned} A_1 &= \frac{2\pi\lambda_B}{\sqrt{\kappa^2+q^2}}\left[1 + \frac{\sqrt{\kappa^2+q^2}-q}{\sqrt{\kappa^2+q^2}+q}e^{-2x_0\sqrt{\kappa^2+q^2}}\right], \\ A_2 &= \frac{2\pi\lambda_B}{\sqrt{\kappa^2+q^2}}, \\ B_2 &= \frac{2\pi\lambda_B}{\sqrt{\kappa^2+q^2}}\left[\frac{\sqrt{\kappa^2+q^2}-q}{\sqrt{\kappa^2+q^2}+q}\right]e^{-2x_0\sqrt{\kappa^2+q^2}}, \\ A_3 &= 4\pi\lambda_B\frac{e^{-x_0\sqrt{\kappa^2+q^2}}}{\sqrt{\kappa^2+q^2}+q}. \end{aligned} \tag{A7}$$

The electrostatic potential in the real space is obtained from the inverse Fourier transform,

$$\phi(s,x) = \frac{1}{2\pi}\int_0^\infty dq\, q J_0(qs)\hat{\phi}(q,s). \tag{A8}$$

APPENDIX B: EFFECTIVE WALL-CHARGE INTERACTION $w(x)$

Using Eqs. (A7) and (A8), we calculate the work $w(x)$ of bringing a point charge from a bulk solution to a distance x from a neutral planar wall.

The potential energy difference at the location of a point charge as it approaches a wall is $\Delta\phi(x_0) = \phi(0, x_0) - \phi(0, \infty)$, which after Fourier transformation becomes

$$\Delta\hat{\phi}(x_0) = \frac{2\pi\lambda_B}{\sqrt{\kappa^2+q^2}}\left[\frac{\sqrt{\kappa^2+q^2}-q}{\sqrt{\kappa^2+q^2}+q}\right]e^{-2x_0\sqrt{\kappa^2+q^2}}. \tag{B1}$$

Using Eq. (A8) for $s = 0$ and transforming the results back to real space yield

$$\Delta\phi(x_0) = \kappa\lambda_B\left[\frac{(1+\kappa x_0)^2 e^{-2\kappa x_0}}{2\kappa^3 x_0^3} - \frac{K_2(2\kappa x_0)}{\kappa x_0}\right]. \tag{B2}$$

To relate the above quantity to work $w(x)$, we use the Debye charging process, which is the special case of thermodynamic integration. Since within the DH $\Delta\phi(x_0)$ is proportional to the charge of a particle at x_0 as $\Delta\phi(x_0; z) = z\Delta\phi(x_0; 1)$, where z is the valance number of the particle, the work associated with charging a particle is $\beta w(x_0) = \int_0^1 dz\,\Delta\phi(x_0; z) = \frac{1}{2}\Delta\phi(x_0; 1)$. This yields

$$\beta w(x) = \frac{\kappa\lambda_B}{2}\left[\frac{(1+\kappa x)^2 e^{-2\kappa x}}{2\kappa^3 x^3} - \frac{K_2(2\kappa x)}{\kappa x}\right]. \tag{B3}$$

APPENDIX C: ELECTROSTATIC INTERACTIONS BETWEEN ADSORBED CHARGES

Electrostatic interactions between adsorbed charges correspond to the Fourier transformed potential,

$$\hat{\phi}(q,0) = \frac{4\pi\lambda_B}{\sqrt{\kappa^2+q^2}+q} \tag{C1}$$

since $x_0 = x = 0$. Using Eq. (A8), we get

$$\phi(s,0) = 2\lambda_B \int_0^\infty dq\, \frac{qJ_0(qs)}{\sqrt{\kappa^2+q^2}+q}, \tag{C2}$$

and after transforming into the real space, we get

$$\phi(s,0) = 2\kappa\lambda_B\left(\frac{1-e^{-\kappa s}-\kappa s e^{-\kappa s}}{\kappa^3 s^3}\right). \tag{C3}$$

The pair interaction between two adsorbed point charges is simply $u(s) = \phi(s,0)$. This leads to

$$\beta u(s) = 2\kappa\lambda_B\left(\frac{1-e^{-\kappa s}-\kappa s e^{-\kappa s}}{\kappa^3 s^3}\right), \tag{C4}$$

where s is the distance between the two adsorbed charges.

APPENDIX D: COARSE-GRAINED ESTIMATE OF U

An approximate way to evaluate the quantity U defined in Eq. (24) is by using the coarse-graining procedure,

$$\sum_{i=2}^{\infty}{}' u(r_{1j}) \to 2\pi\sigma_A \int_R^\infty dr\, r u(r),$$

where σ_A is the surface density of lattice sites and R is the radius of a circle that subtracts the self-interaction of an adsorbed charge with itself and that satisfies $\sigma_A = 1/\pi R^2$. If a is a lattice size, then both σ_A and R can be expressed as

$$\sigma_A = \frac{g_l}{a^2}, \quad R = a\sqrt{\frac{1}{\pi g_l}},$$

where g_l is the dimensionless geometric factor corresponding to a specific lattice. For the square- and hexagonal-lattices, these factors are

$$g_l = 1, \quad g_l = \sqrt{\frac{4}{3}}, \tag{D1}$$

respectively. The course-grained U evaluates to

$$\beta U \approx \frac{2\kappa\lambda_B}{\kappa^3 a^3}\, 2(\pi g_l)^{3/2}\left[1-e^{-\kappa a/\sqrt{\pi g_l}}\right], \tag{D2}$$

where U is shown to be screened algebraically with κ like $U \propto \kappa^{-3}$.

If instead of using the electrostatic potential in Eq. (18) one assumed the screened Coulomb potential $\beta u^{sc}(r) = \lambda_B e^{-\kappa r} r^{-1}$ for the interactions between surface charges, then one would get a drastically different screening behavior,

$$\beta U^{sc} \approx \frac{2\kappa\lambda_B}{\kappa^2 a^2}\, \pi g_l\, e^{-\kappa a/\sqrt{\pi g_l}},$$

which decays exponentially with κ.

APPENDIX E: ELECTROSTATIC INTERACTION BETWEEN AN ADSORBED CHARGE AND A POINT CHARGE AT AN INSULATOR PHASE

If a point charge is located inside an insulator, then the Debye–Hückel equations for the two regions are

$$\begin{aligned} \nabla^2\phi(x,s) &= \kappa^2\phi(x,s) \quad \text{if } x>0 \\ \nabla^2\phi(x,s) &= -4\pi\lambda_B\delta(x-x_0)\frac{\delta(s)}{2\pi s} \quad \text{if } x<0, \end{aligned} \tag{E1}$$

which after Fourier transformation become

$$\begin{aligned} \hat{\phi}''(q,x) &= \left(\kappa^2+q^2\right)\hat{\phi}(q,x), \\ \hat{\phi}''(q,x) &= q^2\hat{\phi}(q,x) - 4\pi\lambda_B\delta(x-x_0), \end{aligned} \tag{E2}$$

and the general solutions in each region are

$$\begin{aligned} \hat{\phi}(q,x>0) &= A_1 e^{-x\sqrt{\kappa^2+q^2}}, \\ \hat{\phi}(q,x<0) &= A_2 e^{(x+h)q} + B_2 e^{-(x+h)q}, \\ \hat{\phi}(q,x<-h) &= A_3 e^{(x+h)q}. \end{aligned} \tag{E3}$$

The continuity of the potential yields

$$\begin{aligned} A_1 &= A_2 e^{hq} + B_2 e^{-hq}, \\ A_3 &= A_2 + B_2, \end{aligned} \tag{E4}$$

and the continuity of the field yields two more relations

$$\begin{aligned} -A_1\sqrt{\kappa^2+q^2} &= A_2 q e^{hq} - B_2 q e^{-hq}, \\ A_3 &= A_2 - B_2 + \frac{4\pi\lambda_B}{q}. \end{aligned} \tag{E5}$$

The four coefficients evaluate as

$$\begin{aligned} A_3 &= \frac{2\pi\lambda_B}{q}\left[1+\frac{q-\sqrt{\kappa^2+q^2}}{q+\sqrt{\kappa^2+q^2}}e^{-2hq}\right], \\ B_2 &= \frac{2\pi\lambda_B}{q}, \\ A_2 &= \frac{2\pi\lambda_B}{q}\left[\frac{q-\sqrt{\kappa^2+q^2}}{q+\sqrt{\kappa^2+q^2}}\right]e^{-2hq}, \\ A_1 &= 4\pi\lambda_B\frac{e^{-hq}}{q+\sqrt{\kappa^2+q^2}}. \end{aligned} \tag{E6}$$

The electrostatic potential for an adsorbed charge is

$$\beta w_c(h) = \phi(0,0) = 2\lambda_B\int_0^\infty dq\, \frac{qe^{-hq}}{\sqrt{\kappa^2+q^2}+q}, \tag{E7}$$

which evaluates to

$$\beta w_c(h) = \frac{2\kappa\lambda_B}{3} + \pi\frac{\lambda_B}{h}\left(Y_2[\kappa h] - H_2[\kappa h]\right) + \frac{4\kappa\lambda_B}{\kappa^3 h^3}. \tag{E8}$$

DATA AVAILABILITY

The data that support the findings of this study are available from the corresponding author upon reasonable request.

REFERENCES

[1]B. Binks and T. S. Horozov, *Colloidal Particles at Liquid Interfaces* (Cambridge University Press, Cambridge, 2006).

[2]F. H. Stillinger, "Interfacial solutions of the Poisson–Boltzmann equation," J. Chem. Phys. **35**, 1584 (1961).

[3]A. J. Hurd, "The electrostatic interaction between interfacial colloidal particles," J. Phys. A: Gen. Phys. **18**, L1055 (1985).

[4]R. R. Netz, "Debye–Hückel theory for slab geometries," Eur. Phys. J. E **3**, 131 (2000).

[5]Y. Levin and J. E. Flores-Mena, "Surface tension of strong electrolytes," Europhys. Lett. **56**, 187 (2001).

[6]D. Frydel, S. Dietrich, and M. Oettel, "Charge renormalization for effective interactions of colloids at water interfaces," Phys. Rev. Lett. **99**, 118302 (2007).

[7]B. W. Ninham and V. A. Parsegian, J. Theor. Biol. **31**, 405 (1971).

[8]B. Honig and A. Nicholls, "Classical electrostatics in biology and chemistry," Science **268**, 1144 (1995).

[9]M. Borkovec, J. Daicic, and G. J. M. Koper, "On the difference in ionization properties between planar interfaces and linear polyelectrolytes," Proc. Natl. Acad. Sci. U. S. A. **94**, 3499 (1997).

[10]R. C. van Duijvenbode, M. Borkovec, and G. J. M. Koper, "Ionization properties of interfaces and linear polyelectrolytes: A discrete charge ising model," Physica A **298**, 1 (1998).

[11]G. J. M. Koper and M. Borkovec, "Proton binding by linear, branched, and hyperbranched polyelectrolytes," Polymer **51**, 5649 (2010).

[12]T. Markovich, D. Andelman, and R. Podgornik, "Complex fluids with mobile charge-regulating macro-ions," Europhys. Lett. **113**, 26004 (2016).

[13]Y. Avni, T. Markovich, R. Podgornik, and D. Andelman, "Charge regulating macro-ions in salt solutions: Screening properties and electrostatic interactions," Soft Matter **14**, 6058 (2018).

[14]R. Podgornik, "General theory of charge regulation and surface differential capacitance," J. Chem. Phys. **149**, 104701 (2018).

[15]D. Frydel, "General theory of charge regulation within the Poisson-Boltzmann framework: Study of a sticky-charged wall model," J. Chem. Phys. **150**, 194901 (2019).

[16]D. Frydel, "One-dimensional Coulomb system in a sticky wall confinement: Exact results," Phys. Rev. E **100**, 042113 (2019).

[17]A. Bakhshandeh, D. Frydel, A. Diehl, and Y. Levin, "Charge regulation of colloidal particles: Theory and simulations," Phys. Rev. Lett. **123**, 208004 (2019).

[18]Y. Avni, D. Andelman, and R. Podgornik, "Charge regulation with fixed and mobile charged macromolecules," Curr. Opin. Electrochem. **13**, 70 (2019).

[19]A. Bakhshandeh, D. Frydel, and Y. Levin, "Charge regulation of colloidal particles in aqueous solutions," Phys. Chem. Chem. Phys. **22**, 24712 (2020).

[20]Y. Avni, R. Podgornik, and D. Andelman, "Critical behavior of charge-regulated macro-ions," J. Chem. Phys. **153**, 024901 (2020).

[21]T. Markovich, D. Andelman, and R. Podgornik, in *Handbook of Lipid Membranes*, edited by C. Safinya and J. Raedler (Taylor & Francis, 2020), Chap. 9.

[22]R. J. Baxter, "Percus–Yevick equation for hard spheres with surface aadhesion," J. Chem. Phys. **49**, 2770 (1968).

[23]I. Langmuir, "The adsorption of gases on plane surface of glass, mica and platinum," J. Am. Chem. Soc. **40**, 1361 (1918).

[24]D. Chakraborty and P. K. Chattaraj, "Bonding, reactivity, and dynamics in confined systems," J. Phys. Chem. **123**, 4513 (2019).

[25]R. G. Smits, G. J. M. Koper, and M. Mandel, "The influence of nearest-neighbor and next-nearest-neighbor interactions on the potentiometric titration of linear poly(ethylenimine)," J. Phys. Chem. **97**, 5745 (1993).

[26]L. D. Roelofs, *Phase Transitions and Kinetics of Ordering in Physical Structure of Solid Surfaces*, edited by N. Unertl (Elsevier, Amsterdam, 1996), p. 713.

[27]D. Andelman, F. Broçhard, and J. F. Joanny, "Phase-transitions in Langmuir monolayers of polar-molecules," J. Chem. Phys. **86**, 3673 (1987).

[28]M. M. Hurley and S. J. Singer, "Domain energies of the dipolar lattice gas," J. Phys. Chem. **96**, 1938 (1992).

[29]M. M. Hurley and S. J. Singer, "Phase transitions at zero temperature in the dipolar lattice gas," J. Phys. Chem. **96**, 1951 (1992).

[30]M. M. Hurley and S. J. Singer, "Domain array melting in the dipolar lattice gas," Phys. Rev. B **46**, 5783 (1992).

[31]A. Majee, M. Bier, and R. Podgornik, "Spontaneous symmetry breaking of charge-regulated surfaces," Soft Matter **14**, 985 (2018).

[32]L. Koopal, W. Tan, and M. Avena, "Equilibrium mono- and multicomponent adsorption models: From homogeneous ideal to heterogeneous non-ideal binding," Adv. Colloid Interface Sci. **280**, 102138 (2020).

[33]G. Barbero, L. R. Evangelista, and I. Lelidis, "Effective adsorption energy and generalization of the Frumkin–Fowler–Guggenheim isotherm," J. Mol. Liq. **320**, 114795 (2020).

[34]D. Frydel, "Mean field electrostatics beyond the point charge description," Adv. Chem. Phys. **160**, 209 (2016).

[35]T. D. Lee and C. N. Yang, , Phys. Rev. **87**, 404 (1952).

[36]H. E. Stanley, *Introduction to Phase Transitions and Critical Phenomena* (Oxford University Press, 1971).

[37]N. Adžić and R. Podgornik, "Field-theoretic description of charge regulation interaction," Eur. Phys. J. E **37**, 49 (2014).

[38]E. M. Wright, "Stability criteria and the real roots of a transcendental equation," SIAM J. Appl. Math. **9**, 136 (1961).

[39]C. E. Siewert and E. E. Burniston, "Solutions of the equation $ze^z = a(z + b)$," J. Math. Anal. Appl. **46**, 329 (1974).

[40]I. Mezõ and G. Keady, "Some physical applications of generalized Lambert functions," Eur. J. Phys. **37**, 065802 (2016).

[41]I. Mezõ and Á. Baricz, "On the generalization of the Lambert W function," J. Trans. Am. Math. Soc. **369**, 7917 (2017).

[42]L. Onsager, "Crystal statistics. I. A two-dimensional model with an order-disorder transition," Phys. Rev. **65**, 117 (1944).

[43]Y. Levin, "Electrostatic correlations: From plasma to biology," Rep. Prog. Phys. **65**, 1577 (2002).

[44]D. A. Skoog, D. M. West, F. J. Holler, and S. R. Crouch, *Fundamentals of Analytical Chemistry*, 9th ed.; International ed. (Brooks/Cole, Cengage Learning, 2014).

[45]A. Naji and R. Podgornik, "Quenched charge disorder and Coulomb interactions," Phys. Rev. E **72**, 041402 (2005).

[46]R. Podgornik and A. Naji, "Electrostatic disorder-induced interactions in inhomogeneous dielectrics," Europhys. Lett. **74**, 712 (2006).

[47]A. Naji, D. S. Dean, J. Sarabadani, R. R. Horgan, and R. Podgornik, "Fluctuation-Induced interaction between randomly charged dielectrics," Phys. Rev. Lett. **104**, 060601 (2010).